25th ABCM International Congress of Mechanical Engineering
October 20-25, 2019, Uberlândia, MG, Brazil

COBEM2019-2418
ENGINEERING Ti-35Nb-Sn ALLOYS WITH GRADED ELASTIC MODULUS BY LASER MELTING FOR BIOMEDICAL APPLICATIONS

Juliane Ribeiro da Cruz
Mechanical Engineering Department, Aeronautics Institute of Technology (ITA), Praça Marechal Eduardo Gomes, 50, 12228-900, São José dos Campos, Sao Paulo, Brazil
juliane.rcruz@gmail.com

Rodnei Bertazzoli
Faculty of Mechanical Engineering, State University of Campinas, Mendeleyev, 200, 13083-860, Campinas, São Paulo, Brazil
rbertazzoli@fem.unicamp.br

Abstract. *To minimize the stress-shielding of bones, implants with low elastic modulus are necessary. However, this eventually leads to an increase in implant-bone shear stresses, that can compromise the implant success. Simulations consistently indicate that optimum implant design requires a structure with variable Young's modulus. In this work, we wish to engineer Ti-35Nb-(0, 2 and 4)Sn mass% alloys with graded elastic modulus by laser melting. Cold-rolled 2 mm thick plates of the three alloys were laser melted. Microstructure characterization was carried out on the melted track transverse cross-section by optical and electron microscopy, x-ray diffraction, EBSD analysis, nanoindentation analysis and Vickers microhardness measurements. Thermal simulation under high heating rates with simultaneous synchrotron x-ray diffraction was performed to assess phase transformations. Results show that cold-rolling promoted the formation of stress-induced α"-martensite with strong <010>α" texture in Ti-35Nb and Ti-35Nb 2Sn alloys. In addition, Ti-35Nb 2Sn alloy also developed {001}⟨100⟩β texture, with low β-phase stability. This resulted in an initial Young's modulus of 57 GPa and 52 GPa, respectively. With laser melting, elastic modulus was locally increased up to 78 GPa, in Ti-35Nb alloy, and up to 72 GPa. in Ti-35Nb-2Sn alloy. This was associated to martensitic reversion and reduction of {001}⟨100⟩β texture with recrystallization. On the other hand, Ti-35Nb-4Sn alloy presented higher β phase stability, developed an initial elastic modulus of 65 GPa, and was not significantly affected by laser melting. Results show that laser melting can effectively produce Ti-35Nb and Ti-35Nb-2Sn implants with graded elastic modulus.*

Keywords: *β Ti alloy, Laser welding, Low elastic modulus, Functionally graded properties*

1. INTRODUCTION

With the increase in population aging and the higher demand for artificial instruments to replace or reconstruct dysfunctional hard tissues, biomedical materials have gained increasing attention in the past decades. Titanium and its alloys have been widely used for these applications because of their high strength-to-ductility ratio, corrosion resistance and excellent biocompatibility (Zhang and Chen, 2019). However, these alloys were not yet entirely suited to this application due to the elastic modulus mismatch between the implant (about 110GPa, for pure Ti and Ti-6Al-4V) and the bone (10-30 GPa, for cortical bone). The higher elastic modulus of implant would prevent load transfer to the bone, that is necessary for bone remodeling. This would eventually lead to bone resorption and implant loosening (Apostu, 2017). To minimize this stress-shielding effect, Ti alloys with lower elastic modulus have been developed (Zhang and Chen, 2019; Niinomi and Nakai, 2011). This new Ti alloys have Ti-β phase at environmental temperature, and present Young´s modulus values typically below 80 GPa.

Ti-35Nb-4Sn is among β-type Ti alloys and has one of the lowest values of Young's modulus reported, about 40 GPa (Jung et. al, 2010, Guo et. al, 2015). This is much closer to that of human cortical bone than other currently used alloys (Zhang and Chen, 2019; Niinomi and Nakai, 2011). However, the achievement of such low elastic modulus requires appropriate chemical composition and specific processing route (Guo et. al, 2015). In Ti-35Nb-4Sn alloy, Nb additions of about 35wt% meta-stabilize Ti-β phase at room temperature, while Sn additions suppress or retard ω phase precipitation, that notably increase the elastic modulus (Cai et al., 2019). As elastic modulus decreases with the stability of β phase (Hou et al., 2016), alloys with lower contents of Nb and Sn (β stabilizers) are also being studied (Hou et al., 2016, Cremasco et al. 2016, Guo et. al, 2015, Dalmau et al. 2015, Hayama et al., 2014). Practical observations have

shown that heavy rolling of Ti-Nb alloy leads to Young´s modulus anisotropy, associated to the formation and stabilization of stress induced α"-martensite (orthorhombic) from the parent β phase (bcc) (Inamura et al., 2005; Matsumoto et al., 2005; Fukui et al., 2004). Results show that the development of <010>α″ and <110> β rolling textures promote Young´s modulus reduction along rolling direction (Hanada et al., 2013; Matsumoto et al., 2007; Matsumoto et al., 2005). Although the reason for elastic modulus reduction with the development of <010>α″ texture is not yet entirely understood, it is speculated that it is related to an increase in interatomic distance of bα" lattice parameter with lattice expansion on β to α" transformation (Matsumoto et al. 2007, Matsumoto et al. 2005). Besides α"-martensite texture, β phase texture also plays an important role in the resulting elastic modulus of these alloys. Studies on the Young's modulus of single crystals (Zhang et al., 2013) and textured β-Ti alloys (Inamura et al., 2005) indicate that the elastic modulus is the lowest in [001]β, and increases in the order of [001]β <[110] β <[lll] β. This is coherent with Hou et al. (2016) investigations on the ultralow Young's modulus of 36 GPa of Ti–33Nb–4Sn, reported by Guo et al. (2015). Hou et al. (2016) attributed such low elastic modulus to the much lower β-phase stability regarding to {001}⟨100⟩β shear (C_{44}), in addition to the a slightly lower β-phase stability with respect to {110}<10> β shear (C').

Despite these great advances in the development of biomaterials with low elastic modulus for reduction of the stress-shielding effect, a homogeneous material with low elastic modulus may not meet all structural requirements for an optimum implant design. That is the case of hip replacement stems, in which the use of an isoelastic material with low elastic modulus (like cortical bone) was demonstrated to increase shear stress at the edge of proximal region (neck), increasing the chances of proximal loosening and failure (Kuiper and Huiskes, 1997). In fact, simulations of optimum implant design for different types of prostheses consistently indicate that optimum performance can only be achieved with graded elastic properties within the material (Enab and, 2013; Kuiper and Huiskes, 1997; Hedia et. al, 2005; Oshkour et. al, 2012; Oshkour et. al, 2014; Ramakrishna et. al, 2004; Ganesh et. al, 2005). Therefore, several studies have been currently focusing in the engineering of materials and manufacturing processes for the development of implants with graded properties for biomedical applications (Lima et. al, 2017; Lopes et. Al, 2014; Jung et al. 2010), specially within the field of functionally graded materials (Sola et. al, 2016). Studies on the engineering of Ti alloys with graded mechanical properties include laser additive manufacturing with different chemical compositions (Lima et. Al, 2017) and levels of porosity (Traini et al., 2008) and laser surface melting (Fanton, 2016). Graded elastic modulus in Ti-Nb-Sn alloy have been obtained by localized aging due to martensite reversion (Jung et al. 2010) and α phase precipitation (Lopes et. Al, 2014; Jung et al. 2010) and, by laser surface melting, due to recovery of severely cold-rolled microstructure (Fanton, 2016). Considering the achievement of graded elastic modulus through different chemical compositions, galvanic corrosion could be stablished. Therefore, elastic modulus gradation by thermal treatment is likely to be less detrimental.

The objective of this study is to manufacture Ti-35Nb-(0, 2 and 4)Sn mass% alloys with low elastic modulus by cold-rolling and stabilization of α"-martensite, to engineer Ti-Nb-Sn alloys with graded elastic modulus by laser melting, and to investigate microstructure causes associated to elastic modulus variations.

2. MATERIALS AND METHODS

High purity charges of about 30 g of Ti-35Nb, Ti-35Nb-2Sn and Ti-35Nb-24Sn (mass%) were arc casted under argon atmosphere for at least 10 times. Ingot were cold-swaged to a 10.4 mm diameter and cold rolled to a 9 mm thickness, for standardization. Then, ingots were ultrasonically degreased with acetone, encapsulated in a quartz tube under argon atmosphere, homogenized for the 24h at 1000ºC, and water quenched in iced water by breaking the quartz tube. Solution treated ingots were chemically stripped (1HF: $1HNO_3$: $5H_2O$) for removal of oxides formed during quenching. Ingot were then cold-rolled along 13 passes from 9 to 2 mm (77% reduction) with in between passes cooling by immersion in room temperature water to prevent martensitic reversion. Cold-rolled plates were decreased with acetone, chemically stripped (1HF: $1HNO_3$: $5H_2O$) and ultrasonically cleaned.

Cold-rolled samples of about 16×13×2 mm were laser melted at the transverse direction. An Yb-fiber laser with Gaussian beam, M^2 factor of 9, wavelength of 1080 nm, 50 µm of focal beam radius and 160 mm of focal distance was used. Remelting was performed with 800 W of power, scan speed of 10 mm/s, at a defocusing distance of 5 mm and with a protective helium flow of 30 l/min. The beam radius and power density at the defocused plane were 313 µm and 259 kW/cm^2, respectively.

Microstructure analysis was performed on transverse cross-section of laser melted track after metallographic preparation by cold mounting, grinding up to 1200 grit, intermediate polishing with 1 and 0.3 µm alumina, and final polishing with 0.04 µm colloidal silica. Kroll's etchant (3 ml HF, 6 ml HNO3 and 91ml H2O) was used to reveal microstructure. Microstructure characterization was carried out by optical microscopy (OM) and scanning electron microscopy (SEM). Electron backscatter diffraction (EBSD) was performed in cold-rolled and recrystallized structure of alloys to evaluate changes in β phase texture. EBSD analysis was carried out using ATEX software by Beausir and Fundenberger (2017). The chemical composition was determined by x-ray fluorescence spectroscopy and by energy-dispersive x-ray spectroscopy (EDS). The electron microscopy work has been performed with FEI/THERMO Quanta 650 FEG available at LNNano, Campinas. Phase determination on transverse cross section of cold-rolled alloys was carried out by X-ray diffraction (XRD) analysis covering an area of 1.5×1.5 mm. A multi detector equipment with 255

channels, Cu Kα radiation, 40 mA and 40 kV, parallel x-ray lenses and 2×2 mm crossed slits were used. Samples were scanned from 30 to 90º, with a step size of about 0.0131º per channel (active length of 3.3473º), and a step time of 100 s. Conventional XRD analysis performed with Cu Kα radiation, from 33 to 90º, was also performed on the rolling plane of cold-rolled samples.

Vickers microhardness profile was determined along the transverse cross-section, from fusion zone to base metal, under 100 gf load and every 100 µm, as an average of three rows. Elastic modulus profile was determined by instrumented nanoindentation and calculated from load-displacement curves, according to the method developed by Oliver and Pharr (2004). Measurements were performed from the center of the weld to the base metal using a maximum load of 0.2 gf, pause of 10 s, loading rate of 800 mN/min and unloading rate of 800 mN/min.

Thermal simulation with simultaneous synchrotron X-ray diffraction (SXRD) was performed at the X-ray Scattering and Thermo-Mechanical Simulation (XTMS) experimental station, located at XRD1 beamline at the Brazilian Synchrotron Light Laboratory (LNLS), in Campinas. In the experiment, samples were heated up to 150, 300, 400, 500, and 600ºC at a 500ºC/s rate, in an evacuated chamber at 4×10^{-2} Torr. Heating cycle was followed by quenching with helium flow, with a resulting average cooling rate of 80ºC/s. Each SRXD pattern was capture for 10s at target temperatures, from 30º to 50º. Crossed slits with 0.5 and 2 mm were used. A beam wavelength of 1.033 nm was used. Bowtie specimens with 2 mm thickness were used.

3. RESULTS AND DISCUSSION

Table 1 shows the average chemical composition of the alloys measured by fluorescence spectroscopy. Results confirm that the chemical composition projected for the alloys was successfully achieved. Figure 1 shows optical microscopy of solution treated ingots and Fig. 2 shows XRD measurements on the cross section of solution treated Ti-35Nb and Ti-35Nb-2Sn ingots. XRD analysis of Ti-35Nb-4Sn ingot generated no diffraction pattern, most likely due to its large grain size that make sample alignment difficult, for constructive interferences. From Fig. 1 and Fig. 2 it can be seen that Ti-35Nb ingot was composed of β grains with abundant α”-martensite plates within, while Ti-35Nb-2Sn ingot was mostly composed of β phase with traces of α” martensite, partially transformed during quenching. Fig. 1 shows that Ti-35Nb-4Sn was entirely composed of β phase. Microstructure of the solution treated ingots are coherent with those reported by Cremasco et al. (2016) and Hayama et al (2014), for these same chemical compositions.

Figure 3 shows cross-section of cold-rolled plates of Ti-35Nb, Ti-35Nb-2Sn and Ti-35Nb-4Sn processed by laser melting. Four characteristic zones are identified: (I) cold-rolled base metal, (II) transition zone, (III) recrystallized heat affected zone and (IV) fusion zone. The region denominated transition zone in this work refers to the heterogeneous part of heat affected zone composed of the cold-rolled structure subjected to recovery treatment (annealing below recrystallization temperature) with fine recrystallized grains within. Transition zone is illustrated by the EBSD band contrast image on the cross section of Ti-35Nb-4Sn alloy shown in Fig. 3.

Table 1. Average chemical composition of alloys measured by fluorescence spectroscopy (mass%)

	Ti	**Nb**	**Sn**
Ti-35Nb	64.9 ± 0.5	35.1 ± 0.5	—
Ti-35Nb-2Sn	63.1 ± 0.2	35.0 ± 0.3	1.9 ± 0.2
Ti-35Nb-4Sn	61.5 ± 0.6	34.5 ± 0.5	4.0 ± 0.2

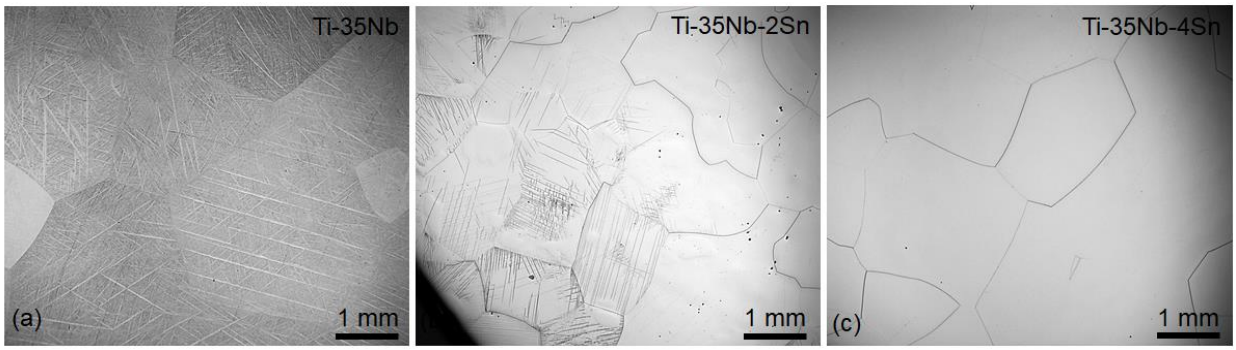

Figure 1. Microstructure analysis of ingots after solution treatment and quenching

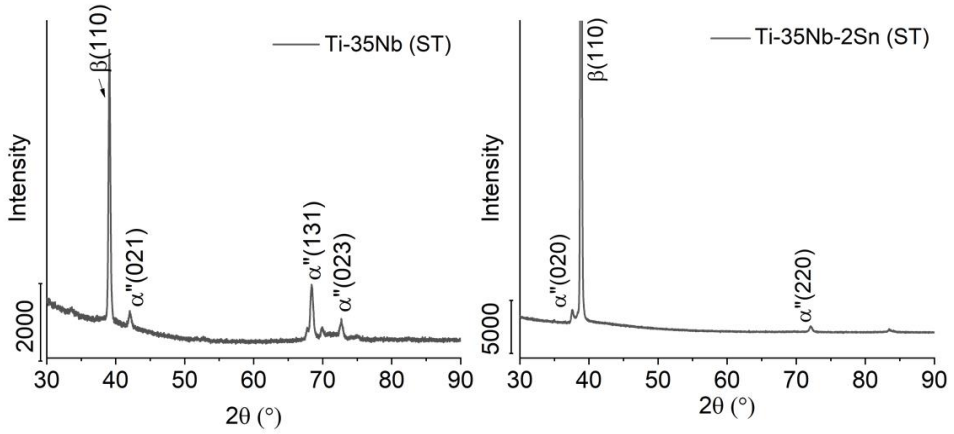

Figure 2. XRD analysis on cross section of solution treated Ti-35Nb and Ti-35Nb-2Sn ingots

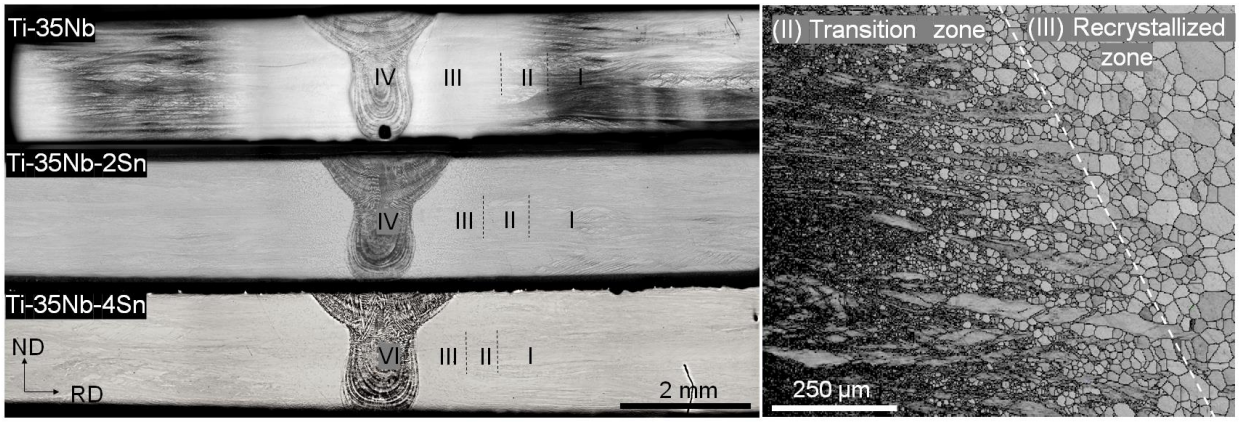

Figure 3. On the left, cross section of laser melted bead along rolling direction showing (I) the cold-rolled base metal, (II) the transition zone, (III) recrystallized zone and (IV) fusion zone. On the right, EBSD map of transition zone on the cross-section of laser melted track of Ti-35Nb-4Sn, alloy along rolling direction

Figure 4 shows microstructure by scanning electron microscopy of fusion zone, recrystallized zone and cold-rolled base metal microstructures. In cold-rolled zone, slip bands structures, typically formed under severe plastic deformation, can be seen. Microstructures of recrystallized zones are similar to those observed in the solution treated alloys (Fig.1), but with smaller grains sizes. While microstructure of Ti-35Nb-4Sn alloy is fully composed of β phase, α" martensite appears in Ti-35Nb and Ti-35Nb-2Sn alloys. The survival of α" martensite in the recrystallized zone of Ti-35Nb and Ti-35Nb-2Sn alloys, indicates that laser melting produces rather a quenching effect than an annealing effect. Studies on annealing of a solution treated Ti-30Nb alloy, composed of β and α" phases, demonstrated that martensite reversion and ω phase precipitation would occur after only one-minute annealing at 400°C (Lopes et al., 2011). However, as laser melting and cooling to room temperature take only a few seconds, such effect associated to annealing was not observed. All alloys presented a dendritic microstructure in fusion zone, in which Nb partitioned to dendritic core and Ti partitioned to interdendritic region, Fig. 5. This agrees with Nb fluctuations reported by Cremasco et al. (2011), in the dendritic structure of a casted Ti-25Nb (mass%) alloy. As Nb additions increase the melting temperature of Ti-Nb alloys, it is coherent that preferential solidification would occur at clusters with higher concentration of Nb, giving rise to dendritic cores enriched with Nb. Consequently, the remaining liquid would progressively have lower contents of Nb. Niobium deprival destabilized β phase in at interdendritic zone, leading to formation of α" martensite in this region. On the other hand, Nb enrichment stabilized β phase in dendritic cores. Although Sn partition was not clearly detected in our analysis, Sn partition to interdendritic region can be expected (Moraes et al., 2014). In Ti-35Nb-4Sn, very little amount of α" martensite was found in interdendritic region, confirming the higher β phase stability of this alloy.

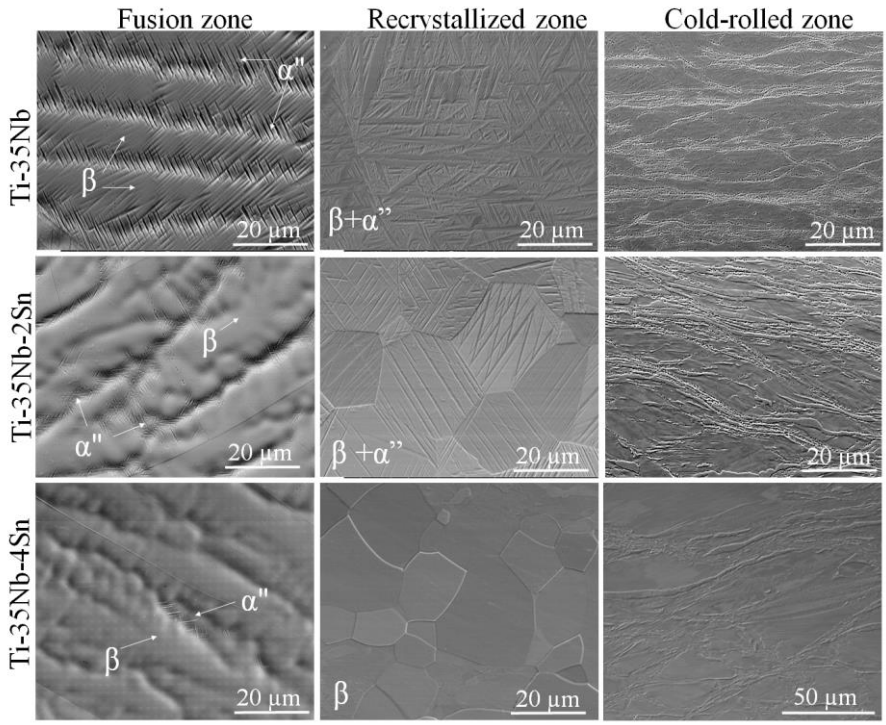

Figure 4. Microstructure of fusion zone, recrystallized heat affected zone and cold-rolled base metal on the cross section of laser melted bead of Ti-35Nb-xSn (0,2 and 4 mass%) alloys

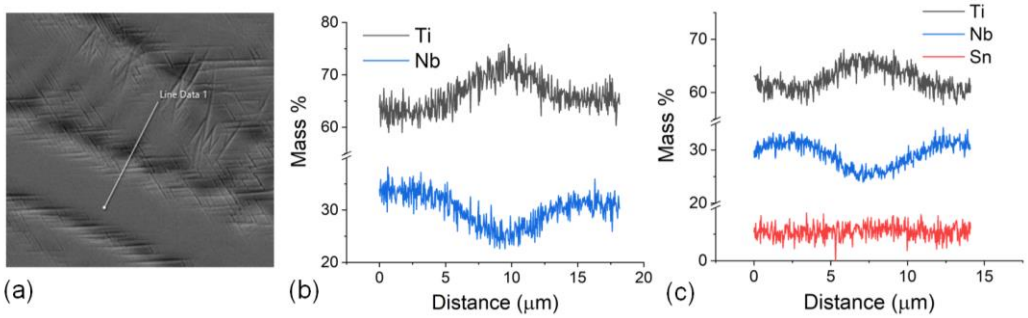

Figure 5. EDS line scan across dendritic structure showing partition of Ti to interdendritic region and of Nb to dendritic core in of fusion zone of (a, b) Ti-35Nb and (c) Ti-35Nb-4Sn

Figure 6 shows the elastic modulus profile and Vickers microhardness profile measured from fusion zone to the cold-rolled base metal. The same scale was used in all graphs for direct comparison. Results show a decrease in microhardness from cold-rolled zone toward transition and recrystallized zone, which is associated to the well know onset of dislocation rearrangement induced by heating, that is maximum under recrystallization. Despite recrystallization, microhardness increase in fusion zone was caused by microstructure refinement promoted by dendritic solidification. Microhardness is maximum at cold-rolled base metal and minimum at recrystallized zone of all alloys. In Ti-35Nb it ranged from about 165 to 210 HV0.1, in Ti-35Nb-2Sn, from 220 to 190 HV0.1 and, in Ti-35Nb-4Sn, from 195 to 170 HV0.1.

In Fig. 6, it is also seen that the alloys developed different elastic modulus profiles with laser melting. While the elastic modulus of Ti-35Nb-4Sn did not show any significant variation with laser melting, the elastic modulus of Ti-35Nb and Ti-35Nb-2Sn alloys was significantly increase in fusion zone and heat affected zone. Young`s modulus measurements in transition zone of these alloys presented high deviation associated to the heterogeneous microstructure of this zone, as shown in Fig. 3. Nevertheless, in transition zone of Ti-35Nb-2Sn alloy, elastic modulus remains placed within those of the adjacent zones. In Ti-35Nb, elastic modulus reaches minimum values at transition zone, following a decrease tendency from measurements performed on cold-rolled base metal. As ω particles, typically nanometric, form in the microstructure of Sn free Ti-Nb alloys (Moraes et al., 2014; Kim et al., 2006), this progressive decrease could be associated to solubilization of any diffusional ω nanoparticles (thermal ω) precipitated during ingot cooling. Average Young's modulus values of fusion zone, recrystallized zone and cold-rolled base metal are shown in Fig. 7a. Measurement performed in transition zone were not included in Fig. 7, as the performance of this region cannot be accurately represented by average values.

It can be seen in Fig. 7 that the alloys had different elastic modulus in the initial (cold-rolled) condition. Ti-35Nb-4Sn alloy had the highest elastic modulus of about 65 GPa, followed by Ti-35Nb, with about 57 GPa, and by Ti-35Nb-2Sn, with about 52 GPa. Differences in the initial Young's modulus of alloys seem to be related to textures evolved during cold-rolling. Fig. 8 shows XRD diffraction patterns of cold-rolled alloys on transverse cross section and on rolling plane. In the transverse cross section of Ti-35Nb and Ti-35Nb-2Sn alloys, the strong (020)α" and (110)β texture suggest the the development of <010>α" and <110>β textures along rolling direction, which has been associated to Young's modulus reduction along rolling direction (Hanada et al., 2013; Matsumoto et al., 2007; Matsumoto et al., 2005). The development of (020)α" peak along deformation direction is coherent with findings from Guo et al. (2017) that reported similar results on tensile tested of solution treated Ti-33Nb-4Sn alloy with low elastic modulus. More specifically, the low Young's modulus of Ti-Nb-Sn alloys has been associated to (200)[010]α" and (220)[001]α" rolling textures, that evolve from {100}<110>β and {211}<110>β textures, respectively, following specific orientation relationship (Matsumoto et al., 2007; Matsumoto et al., 2005). Although the development of (200)α" and (220)α" textures in the rolling plane of the three alloys textures can be a strong indicator of the formation of (220)[001]α" and (200)[010]α" textures, no clear indication of <010>α" texture was seen in transverse cross section Ti-35Nb-4Sn alloy, besides some eccentricity in the base of (110)β peak. The development of strong <010>α" texture in Ti-35Nb and Ti-35Nb-2Sn may be the cause of their lower initial Young's modulus, in comparison to that of Ti-35Nb-4Sn.

After laser melting, average elastic modulus of Ti-35Nb-4Sn remained nearly the same while that of Ti-35Nb and Ti-35Nb-2Sn was increased in about 20 GPa, in fusion zone and in recrystallized regions, Fig. 7a. As Young's modulus did not significantly changed from fusion zone to recrystallized zone, elastic modulus increase must be rather associated to solid state microstructure transformations. To investigate possible phase transformations, high heating rate thermal simulation was performed with simultaneous synchrotron X-ray diffraction analysis at up to 600°C, followed by a final measurement in the end of the test. Results are presented in Fig. 9. Results show that the stress induced α" martensite of Ti-35Nb and Ti-35Nb-2Sn is fully reversed to β phase by heating below 300°C while that of Ti-35Nb-4Sn reverts at a lower temperatures, below 150°C. Such low reversion temperatures could explain the absence of <010>α" texture in Ti-35Nb-4Sn, that could have been reverted by heating induced during cold-rolling. At the end of the test, β phase is retained in Ti-35Nb-2n and Ti-35Nb-4Sn alloy while, in Ti-35Nb, part of β phase partially transforms to α" martensite. The reversion of stress induced martensite with strong <010>α" texture accounts for the Young's modulus increase (Matsumoto et al., 2007), as observed in fusion zone and heat affected zones with laser melting.

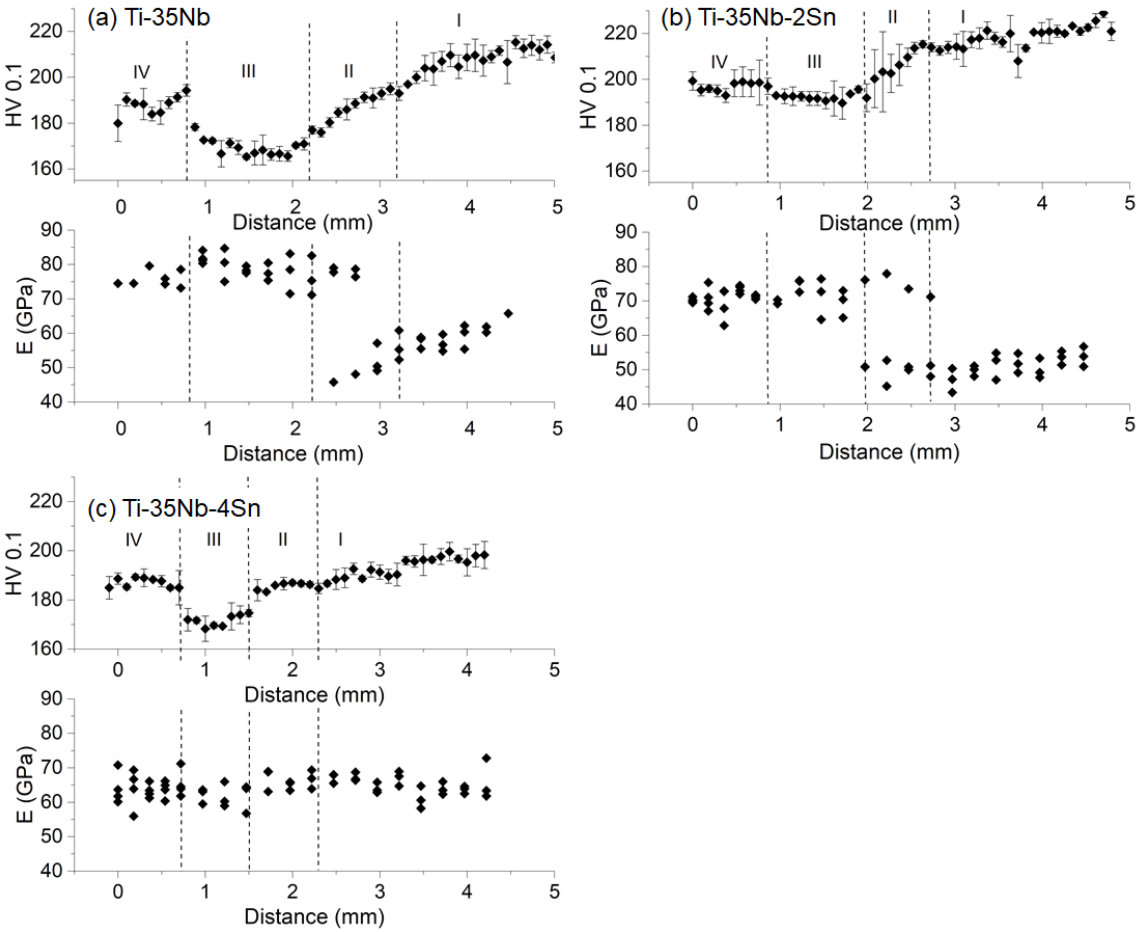

Figure 6. Vickers microhardness and Young' modulus profile from fusion zone to base metal

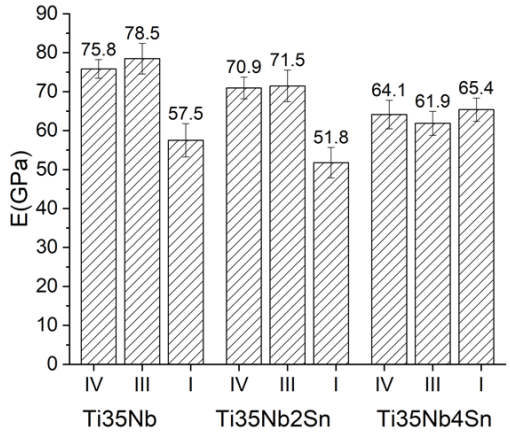

Figure 7. (a) Average Young's modulus E of (I) cold-rolled base metal, (III) recrystallized zone an (IV) fusion zone of Ti-35Nb, Ti-35Nb-2Sn and Ti-35Nb-4Sn alloys

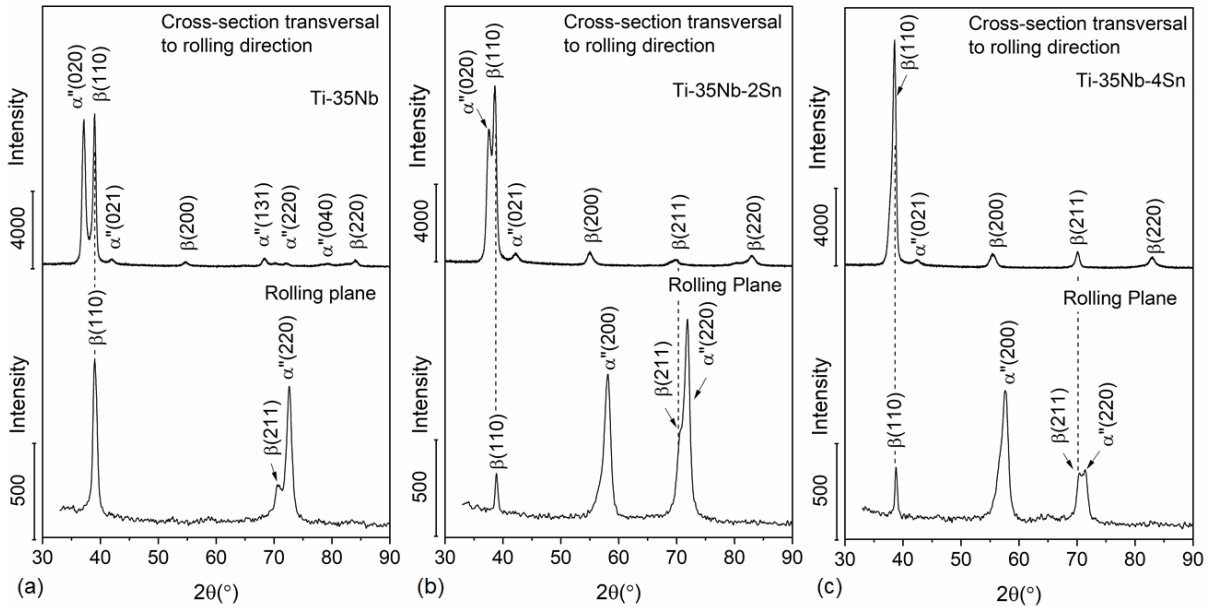

Figure 8. XRD analysis of cold-rolled alloys on transverse cross section and on rolling plane

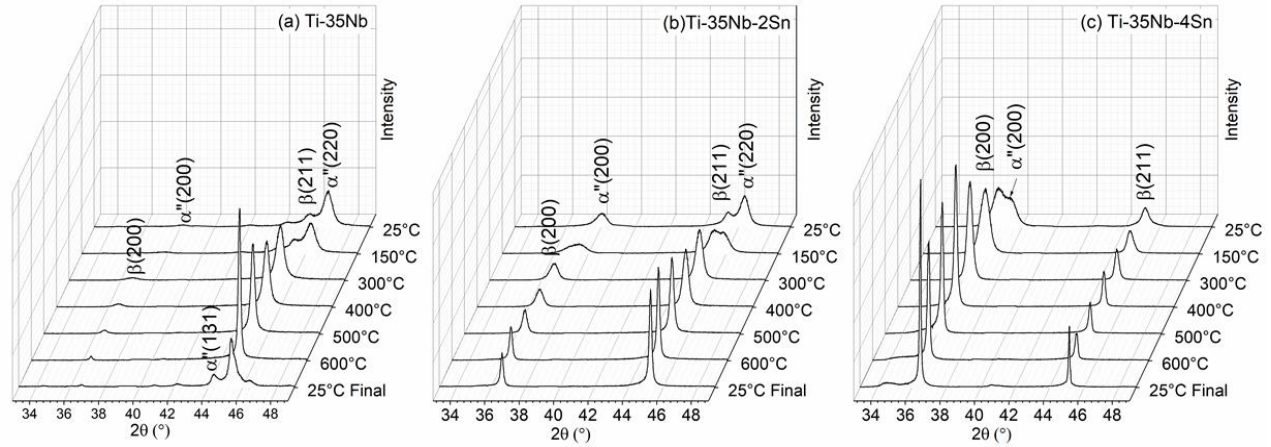

Figure 9. Synchrotron light X-ray diffraction patterns at different temperatures during high heating rate thermal simulation at up to 600°C, and at room temperature in the end of the test

Spots with low Young's modulus measured is transition zone, which indicate that either martensitic transformation was not complete in this region or there are other factors contributing to the low elastic modulus of Ti-35Nb and Ti-35Nb-2n alloys. Fig. 10 shows orientation distribution functions of β phase texture in the cold-rolled and recrystallized condition of alloys, determined by EBSD analysis of these regions. Results show that all alloys developed strong textures along γ fiber, both in cold-rolled and recrystallized zones, which means that grains are oriented so that a {111} plane is parallel to the surface of the sample, perpendicular to normal direction (Yang et al., 2014). In addition, the development of other texture have also been observed. ODF confirmed the development of {112}<110>β texture Ti-35Nb alloy, which is has an orientation relationship with (220)[001]α", reported to evolve in alloys with low young's modulus. In the recrystallized condition this texture becomes stronger due to reversion of (220)[001]α" to the parent {112}<110>β orientations, which is followed by an increase in Young's modulus. In Ti-35Nb-2Sn alloy, although {112}<110>β and {100}<110>β are not observed in the cold-rolled condition, these textures reappear after recrystallization and reversion of strain induced (220)[001]α" and (200)[010]α" to the respective β phase parent orientations. This alloy also developed a strong texture close to {001}<100> in the cold-rolled condition, that was weakened in the recrystallized condition, Fig. 10b. It is known that the Young's modulus decreases with decreasing the β-phase stability (Adbel-Hady et al., 2006). In Ti-33Nb-4Sn alloys with ultralow elastic modulus, it was identified a much lower β phase stability with respect to {001}⟨100⟩β shear (C_{44}) than in other β-Ti alloys (Ti-Cr, Ti-V), which was identified as the main cause of such low elastic modulus (Hou et al. 2016). Therefore, besides the development of stress induced martensite with <010> texture, the development of {001}⟨100⟩β texture, with low β-phase stability, also accounts for the low elastic modulus of about 52 GPa of Ti-35Nb-2Sn alloy in the initial condition. Such texture can also be the cause of the low Young's modulus measurement in transition zone. The weakening of this texture with recrystallization and the reversion of stress-induced martensite contribute to the increase in Young's modulus after laser melting. In Ti-35Nb-4Sn alloy, some texture close to {100}<110>β can be seen in cold-rolled and recrystallized conditions, where it is slightly stronger. Although this texture can be associated with the formation of (200)[010]α", reported to induce elastic modulus reduction along rolling direction, this alloy did not develop <010> α" texture, as seen in Fig. 8c and previous discussed.

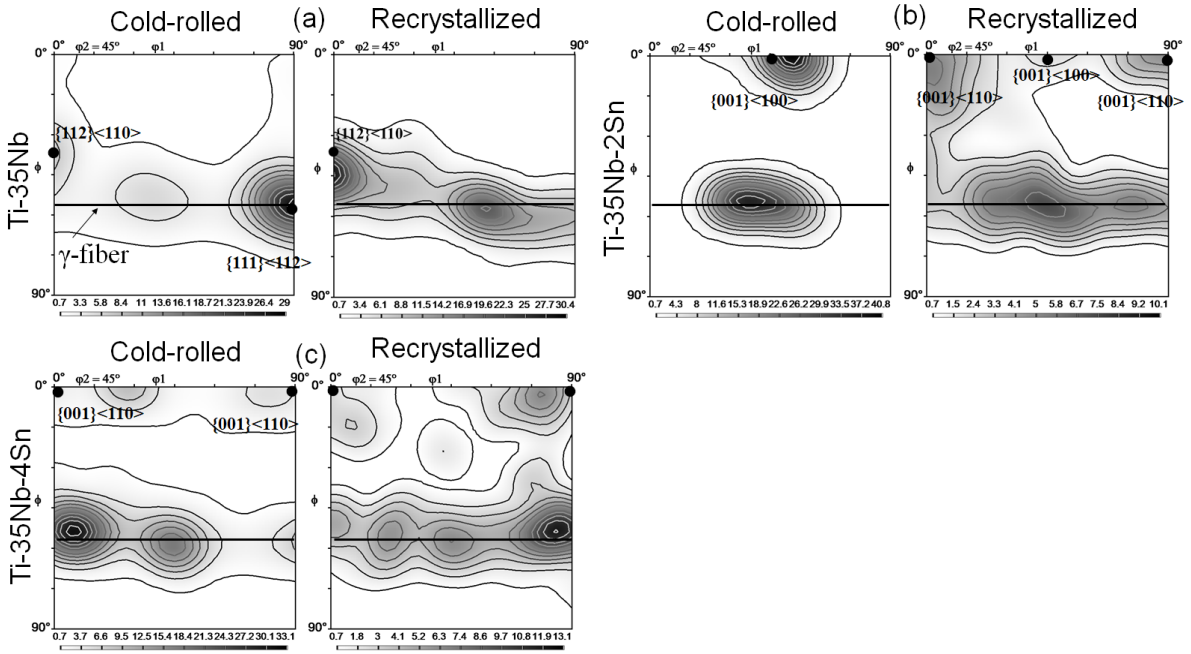

Figure 10. Orientation distribution function at φ=45° of β phase on cold-rolled and recrystallized regions

4. CONCLUSIONS

Laser melting of Ti-35Nb-xSn (x=0, 2 and 4 mass %) cold-rolled plates is proposed to engineer alloys with graded elastic modulus for biomedical application. Mains conclusions are:

The stability of β-phase increase with Sn additions. In Ti-35Nb and Ti-35Nb-2Sn alloys, cold-rolling promoted the formation of stress-induced α"-martensite with strong <010>α" and <110>β texture. Ti-35Nb-2Sn alloy also also developed {001}⟨100⟩β texture, with very low β-phase stability. This resulted in an initial Young's modulus of 57 GPa, for Ti-35Nb, and 52 GPa, for Ti-35Nb-2Sn alloy. Ti-35Nb-4Sn alloy presented the highest β phase stability and an initial elastic modulus of 65 GPa, that was not significantly affected by laser melting.

In Ti-35Nb and Ti-35Nb-2Sn, laser melting promoted localized increase in the elastic modulus (fusion zone and heat affected zone) up to 78 and 72GPa, respectively. In Ti-35Nb this increase was associated with the reversion of

(220)[001]α" texture to {112}<110>β textures. In Ti-35Nb-2Sn, the increase in elastic modulus was followed by reversion of (200)[010]α" texture to {100}<110>β texture and to the weakening of {001}⟨100⟩β texture, with recrystallization.

In all alloys, laser melting promoted recrystallization of heat affected zone, where hardness was decreased, and dendritic solidification at fusion zone, where hardness was reestablished. No significant change is elastic modulus occurred from fusion zone to recrystallized zone. Ti-35Nb-2Sn ally presented the highest microhardness values (190 to 220 HV0.1), which account for a higher mechanical resistance of this alloy.

Results suggest that, in β-Ti alloys with low elastic modulus and strong <010>α" texture, laser melting can effectively be used to fabricate implants with graded elastic modulus.

5. ACKNOWLEDGEMENTS

Authors thank CAPES, for graduation scholarship, and FAPESP, for research funding (Proc. 2016/10637-4). Special thanks to Prof. Dr. Milton Sérgio Fernandes de Lima, for his support with laser processing and EBSD analysis, and to Prof. Dr. Rubens Caram, Dr. Leonardo Fanton, M.Eng. Dalton Daniel de Lima and Dr. Mariana Geradi de Mello for helpful conversations, and support with nanoindentation and fluorescence spectroscopy analysis, and to Dr. Victor Riguetti for his support with x-ray diffraction analysis. Authors thank LNNano/CNPEM/MCTIC for technical support during electron microscopy work. Research supported by LNLS - Brazilian Synchrotron Light Laboratory, CNPEM/MCTIC.

6. REFERENCES

Abdel-Hady, M., Hinoshita, K., Morinaga, M., 2006. "General approach to phase stability and elastic properties of β-type Ti- alloys using electronic parameters". *Scr. Mater.* 55, 477–480.

Apostu D., Lucaciu O., Berce C., Lucaciu D., and Cosma D., 2017. "Current methods of preventing aseptic loosening and improving osseointegration of titanium implants in cementless total hip arthroplasty: a review," *J. Int. Med. Res.*, vol. , no. , p..

Beausir, B. and Fundenberger J.-J., 2017 "Analysis Tools for Electron and X-ray diffraction", ATEX - software, www.atex-software.eu, Université de Lorraine – Metz.

Cai S., Wang L., Schaffer J. E., Gao J., and Ren Y., 2019. "Influence of Sn on martensitic beta Ti alloys," *Mater. Sci. Eng. A*, vol. 743, no. September 2018, pp. 764–772.

Cremasco, A., Lopes, E. S. N., Bertazzoli, R., Caram, R., 2016. "Application of coupled substrate aging and TiO2 nanotube crystallization heat treatments in cold-rolled Ti–Nb–Sn alloys". *Journal of Materials Science*. Vol. 51, No. 13, pp. 6389–6399.

Dalmau, A., Pina, V. G., Devesa, F., Amigó, V., Muñoz, A. I., 2015. "Electrochemical behavior of near-beta titanium biomedical alloys in phosphate buffer saline solution". *Materials Science and Engineering: C*. Vol. 48, pp. 55–62.

Enab, T. A. Enab and Bondok, N. E., 2013. "*Material selection in the design of the tibia tray component of cemented artificial knee using finite element method*" Mater. Des., vol. 44, pp. 454–460.

Fanton L., *Influence of plastic deformation and crystallographic texture on obtaining a stiffness gradient in Ti-30Nb-4Sn alloy by laser surface melting.* PhD thesis. Universidade Estadual de Campinas, Campinas, 2017.

Fukui Y., Inamura T., Hosoda H., Wakashima K., and Miyazaki S., 2004. "Mechanical Properties of a Ti-Nb-Al Shape Memory Alloy," *Mater. Trans.*, vol. 45, no. 4, pp. 1077–1082.

Ganesh V. K., Ramakrishna K., and Ghista D. N., 2005. "Biomechanics of bone-fracture fixation by stiffness-graded plates in comparison with stainless-steel plates.," *Biomed. Eng. Online*, vol. 4, p. 46, 2005.

Guo, S., Meng, Q., Zhao, X., Wei, Q., Xu, H., 2015. "Design and fabrication of a metastable β-type titanium alloy with ultralow elastic modulus and high strength". *Scientific Reports*. Vol. 5, pp. 1-8.

Hanada S., Masahashi N., and Jung T. K., 2013 "Effect of stress-induced α″ martensite on Young's modulus of β Ti-33.6Nb-4Sn alloy," *Mater. Sci. Eng. A*, vol. 588, pp. 403–410.

Hayama, A. O. F., Lopes, J. F. S. C., Gomes da Silva, M. J., Abreu, H. F. G., Caram, R., 2014. "Crystallographic texture evolution in Ti–35Nb alloy deformed by cold rolling". *Materials & Design*. Vol. 60, pp. 653–660.

Hedia H. S., El-Midany T. T., Shabara M. A. N., and Fouda N., 2005 "Development of cementless metal-backed acetabular cup prosthesis using functionally graded material," *Int. J. Mech. Mater. Des.*, vol. 2, no. 3–4, pp. 259–267.

Hou Y. P. et al., 2016 "Origin of ultralow Young's modulus in a metastable β-type Ti-33Nb-4Sn alloy," J. *Mech. Behav. Biomed. Mater*., vol. 59, pp. 220–225.

Inamura T., Hosoda H., Wakashima K., and Miyazaki S.,2005. "Anisotropy and Temperature Dependence of Young's Modulus in Textured TiNbAl Biomedical Shape Memory Alloy," *Mater. Trans.*, vol. 46, no. 7, pp. 1597–1603.

Kuiper J. H. and Huiskes, R., 1997. "Mathematical Optimization of Elastic Properties: Application to Cementless Hip Stem Design," *J. Biomech. Eng.*, vol. 119, no. 2, p. 166.

Jung, T. K., Matsumoto, H., Abumiya, T., Masahashi, N., Kim, M. S., Hanada, S., 2010. "Mechanical Properties-Graded Ti Alloy Implants for Orthopedic Applications". *Materials Science Forum*. Vol. 631–632, pp. 205–10.

Kim, H. Y., Ikehara, Y., Kim, J. I., Hosoda, H. and Miyazaki, S., 2006. "Martensitic transformation, shape memory effect and superelasticity of Ti-Nb binary alloys," *Acta Mater*., vol. 54, no. 9, pp. 2419–2429.

Lima, D. D., Mantri, S.A., Mikler, C. V., Contieri, R., Yannetta, C. J., Campo, K. N., et al., 2017. "Laser additive processing of a functionally graded internal fracture fixation plate". *Materials & Design*. Vol. 130, pp. 8–15.

Lopes E. S. N., Cremasco A., Afonso C. R. M., and Caram R., 2011. "Effects of double aging heat treatment on the microstructure, Vickers hardness and elastic modulus of Ti-Nb alloys" *Mater. Charact*., vol. 62, no. 7, pp. 673–680.

Lopes, E. S. N., Contieri, R. J., Button, S. T., Caram, R., 2015. "Femoral hip stem prosthesis made of graded elastic modulus metastable β Ti Alloy". *Materials & Design*. Vol. 69, pp. 30–36.

Matsumoto H., Watanabe S., and Hanada S., 2005. "Beta TiNbSn Alloys with Low Young’s Modulus and High Strength," *Mater. Trans.*, vol. 46, no. 5, pp. 1070–1078.

Matsumoto, H., Watanabe, S., Hanada, S., 2007. "Microstructures and mechanical properties of metastable β TiNbSn alloys old rolled and heat treated". *Journal of Alloys and Compounds*. Vol. 439, No. 1–2, pp. 146–155.

Moraes, P. E. L., Contieri, R. J., Lopes, E. S. N., Robin, A., and Caram, R., 2014 "Effects of Sn addition on the microstructure, mechanical properties and corrosion behavior of Ti-Nb-Sn alloys," *Mater. Charact*., vol. 96, pp. 273–281.

Niinomi, M., Nakai, M., 2011. "Titanium-Based Biomaterials for Preventing Stress Shielding between Implant Devices and Bone". *International Journal of Biomaterials*. Pp. 1–10.

Oliver, W. C., Pharr, G. M., 2004. "Measurement of hardness and elastic modulus by instrumented indentation: Advances in understanding and refinements to methodology". *Journal of Materials Research*. http://dx.doi.org/10.1557/jmr.2004.19.1.3 Vol.19, No. 1, pp. 3-20.

Oshkour A., Osman N. A. A., Yau Y. H., Tarlochan F., and Abas W. A. B. W., 2013. "Design of new generation femoral prostheses using functionally graded materials: A finite element analysis," *Proc. Inst. Mech. Eng. Part H J. Eng. Med.*, vol. 227, no. 1, pp. 3–17.

Ozaki, T.; Matsumoto, H.; Miyazaki, T.; Hasegawa, M.; Watanabe, S.; Hanada, S., 2005. "Development of beta titanium alloys with low Young's modulus". *Adv. Mater. Process*. Vol. 163, pp. 68–70.

Ramakrishna K., Sridhar I., Sivashanker S., Khong K. S., and Ghista D. N., 2005. "Design of Fracture Fixation Plate for Necessary and Sufficient Bone Stress Shielding," *JSME Int. J. Ser. C*, vol. 47, no. 4, pp. 1086–1094, 2005.

Sola A., Bellucci D., and Cannillo V., 2016, "Functionally graded materials for orthopedic applications – an update on design and manufacturing," *Biotechnol. Adv.*, vol. 34, no. 5, pp. 504–531.

Traini, T., Mangano, C., Sammons, R.L., Mangano, F., Macchi, A., Piattelli, A., 2008. "Direct laser metal sintering as a new approach to fabrication of an isoelastic functionally graded material for manufacture of porous titanium dental implants". *Dental Materials*. Vol. 24, No. 11, pp. 1525–33.

Yang Y., Castany P., Cornen M., Thibon I., Prima F., and Gloriant T., 2014. "Texture investigation of the superelastic Ti-24Nb-4Zr-8Sn alloy," *J. Alloys Compd*., vol. 591, pp. 85–90.

Zhang L. C. and Chen L. Y., 2019 "A Review on Biomedical Titanium Alloys: Recent Progress and Prospect," *Adv. Eng. Mater.*, vol. 21, no. 4, pp. 1–29.

Zhang Y.W., Li S.J., Obbard E.G., Wang H., Wang S.C., Hao Y.L., Yang R., 2011. "Elastic properties of Ti–24Nb–4Zr–8Sn single crystals with bcc crystal structure" *Acta Mater*. Vol. 59, pp. 3081–3090.

7. RESPONSIBILITY NOTICE

The authors are the only responsible for the printed material included in this paper.